
K-MEANS AS A RADIAL BASIS FUNCTION NETWORK: A VARIATIONAL AND GRADIENT-BASED EQUIVALENCE

Felipe de Jesús Félix Arredondo
School of Engineering and Sciences
Tecnológico de Monterrey
Monterrey, Mexico
ffelix3ro@gmail.com

Manuel Alejandro Ucan Puc
School of Engineering and Sciences
Tecnológico de Monterrey
Monterrey, Mexico
Alejandro.ucan-puc@tec.mx

Carlos Astengo Noguez
School of Engineering and Sciences
Tecnológico de Monterrey
Guadalajara, Mexico
castengo@tec.mx

March 6, 2026

ABSTRACT

This work establishes a rigorous variational and gradient-based equivalence between the classical K-Means algorithm and differentiable Radial Basis Function (RBF) neural networks with smooth responsibilities. By reparameterizing the K-Means objective and embedding its distortion functional into a smooth weighted loss, we prove that the RBF objective Γ -converges to the K-Means solution as the temperature parameter σ vanishes. We further demonstrate that the gradient-based updates of the RBF centers recover the exact K-Means centroid update rule and induce identical training trajectories in the limit. To address the numerical instability of the Softmax transformation in the low-temperature regime, we propose the integration of Entmax-1.5, which ensures stable polynomial convergence while preserving the underlying Voronoi partition structure. These results bridge the conceptual gap between discrete partitioning and continuous optimization, enabling K-Means to be embedded directly into deep learning architectures for the joint optimization of representations and clusters. Empirical validation across diverse synthetic geometries confirms a monotone collapse of soft RBF centroids toward K-Means fixed points, providing a unified framework for end-to-end differentiable clustering.

Keywords K-Means, Radial Basis Function (RBF) Networks, Γ -convergence, End-to-end differentiable clustering, Entmax-1.5, Variational equivalence, Joint optimization, Gradient dynamics

1 Introduction

K-Means remains one of the most widely used clustering algorithms due to its simplicity, closed-form centroid updates, and near-linear computational cost [Arthur and Vassilvitskii, 2006b, Kanungo et al., 2002]. Its limitation is not algorithmic but structural: hard assignments induce non-differentiable Voronoi partitions, which prevents K-Means from being directly embedded into end-to-end gradient-based optimization pipelines. As a result, K-Means is usually treated as an external discrete procedure rather than as part of a continuous learning system.

These structural limitations often push K-Means toward poor local minima in heterogeneous datasets. While alternative methods, such as density-based or spectral clustering, mitigate these failures by relaxing geometric assumptions [Ginés-Palestino et al., 2025, Ahmed et al., 2020, Schubert, 2023], our work focuses on reconciling the computational gap between K-Means and differentiable RBF networks.

Radial Basis Function (RBF) networks, on the other hand, optimize their centers through smooth, distance-based activations and are fully compatible with gradient descent [Moody and Darken, 1989, Park and Sandberg, 1991]. Despite this, their relationship with K-Means is often described as an approximation or a heuristic relaxation [Xu and Jordan, 1996], but heuristics lack guarantees of convergence. Previous work has explored related connections from a probabilistic perspective, showing that K-Means can be interpreted as a variational EM approximation to Gaussian

mixture models with isotropic covariances [Lücke and Forster, 2019]. These approaches establish a link between hard clustering and soft probabilistic assignments within the EM framework.

This dichotomy raises a fundamental question: can K-Means itself be characterized as a differentiable model rather than as an external discrete procedure with the RBFs?

We answer this affirmatively from a variational standpoint. Under mild and explicit conditions (formalized in Sections 3.3 and 3.4), the K-Means distortion can be rewritten in terms of responsibility variables and identified with a smooth weighted RBF loss. In this formulation, the RBF functional admits the classical K-Means objective as its Γ -limit as $\sigma \rightarrow 0$, and the corresponding gradient-flow dynamics collapse to the centroid update rule, yielding identical centroid configurations and cluster assignments in the singular limit. K-Means therefore emerges as the zero-temperature regime of a differentiable RBF network, providing a unified optimization framework in which clustering and representation learning are jointly optimized. This perspective is particularly relevant given the known structural limitations of K-Means under heterogeneous data distributions: its reliance on isotropic, Euclidean geometry [Celebi et al., 2013, Ushenko et al., 2025] restricts its ability to represent elongated, anisotropic, or manifold-supported structures, often forcing complex regions to be approximated by multiple spherical components and degrading geometric interpretability [Raykov et al., 2016].

This structural separation reveals a fundamental methodological gap between discrete partitioning and continuous optimization. K-Means induces sharp Voronoi regions through hard assignments and closed-form centroid updates [Telgarsky and Vattani, 2010], producing piecewise-constant decision boundaries, whereas RBF networks define smoothly decaying, overlapping receptive fields optimized via gradient-based dynamics. Although both share a common geometric intuition, their optimization mechanisms are incompatible, which in practice enforces a two-stage pipeline where K-Means initializes centers that are subsequently embedded into a continuous model [Caron et al., 2018]. Interpreting K-Means as the zero-temperature limit of a differentiable RBF formulation resolves this tension within a single variational framework: the clustering objective becomes embedded in a smooth loss whose stationary conditions recover the classical centroid updates, thereby unifying combinatorial partitioning and gradient-based representation learning and enabling coherent joint optimization [Que and Belkin, 2016, Faraoun and Boukelif, 2006, Zhu et al., 2011].

Our main theoretical results are summarized as follows:

Main Contribution. The main theoretical result establishes a variational equivalence between the soft RBF objective and the classical K-Means distortion functional. Specifically, we prove that:

- (i) the RBF loss Γ -converges to the K-Means objective as $\sigma \rightarrow 0$;
- (ii) the gradient dynamics of the RBF centers recover the exact K-Means centroid update; and
- (iii) both formulations generate identical centroid configurations and partitions in the limit.

Consequently, K-Means is characterized as the zero-temperature limit of a differentiable RBF network within a unified optimization framework.

Organization of the Paper. The remainder of the paper is organized as follows. Section 3.3 formalizes the variational equivalence between the RBF loss and the K-Means distortion functional. Section 3.4 analyzes the gradient-flow dynamics and proves recovery of the centroid update rule. Section 4 provides empirical validation across synthetic geometries. Finally, Section 5 discusses implications for end-to-end clustering and hybrid neural architectures.

2 Preliminaries and Theoretical Background

Before establishing the equivalence between K-Means and Radial Basis Function (RBF) models, it is necessary to introduce the mathematical objects that underlie both formulations. Although K-Means is traditionally presented as a discrete clustering algorithm and RBF networks as continuous, differentiable architectures, both rely fundamentally on distance-based representations in Euclidean spaces.

2.1 K-Means

First, we formalize and simplify in order to obtain a representation compatible with later comparisons to RBF-based neural models. The notation adopted follows the generalized formulation introduced in [Arthur and Vassilvitskii, 2006a], and the algorithmic structure remains consistent with the theoretical treatment in [Blömer et al., 2016]. The goal of this section is not to introduce new variants of K-Means, but to express its standard formulation in a way that exposes its underlying optimization structure.

Let $D = \{x_1, \dots, x_n\} \subset \mathbb{R}^d$ be a dataset of n points. The K-Means algorithm seeks a partition of the dataset into k disjoint subsets $S = \{S_1, \dots, S_k\}$ together with a collection of representative points (centroids) $M = \{\mu_1, \dots, \mu_k\} \subset \mathbb{R}^d$.

For each subset S_i , define its empirical variance as

$$\text{Var}(S_i) = \frac{1}{|S_i|} \sum_{x \in S_i} \|x - \mu_i\|^2, \quad (1)$$

where $\mu_i = \frac{1}{|S_i|} \sum_{x \in S_i} x$ denotes the empirical mean of S_i .

The classical K-Means objective consists of minimizing the total within-cluster squared distortion

$$\min_{S_1, \dots, S_k} \sum_{i=1}^k \sum_{x \in S_i} \|x - \mu_i\|^2 = \min_{S_1, \dots, S_k} \sum_{i=1}^k |S_i| \text{Var}(S_i), \quad (2)$$

which penalizes intra-cluster dispersion. The equivalence between both expressions follows directly from the definition of empirical variance.

From this objective, the assignment rule naturally follows:

$$S_i = \{x_j \in D : \|x_j - \mu_i\|^2 \leq \|x_j - \mu_l\|^2, \forall l\}, \quad (3)$$

where i is the cluster and j is the index of the data, and this simply assigns each point to its nearest centroid based on the Euclidean distance between them, which generates the assigned clusters of the data and makes groups determined by the centers. Once the partition is fixed, minimizing (2) with respect to μ_i yields the closed-form update

$$\mu_i = \frac{1}{|S_i|} \sum_{x \in S_i} x, \quad (4)$$

showing that each centroid is the arithmetic mean of the points assigned to it. The algorithm iterates these two steps until convergence, typically defined by a tolerance condition

$$\max_i \|\mu_i^{(t)} - \mu_i^{(t-1)}\| < \tau. \quad (5)$$

or stop after T steps chosen by hand.

2.2 Radial Basis Function Networks and Their Responsibilities

Radial Basis Function (RBF) networks are among the earliest neural architectures grounded in interpolation theory and distance-based modeling [Lowe and Broomhead, 1988, Moody and Darken, 1989, Park and Sandberg, 1991] used to measure distances between centroids extracted from a certain data under a Gaussian perspective. Let $D \subset \mathbb{R}^d$ denote the dataset or a processed latent space, and $x \in D$ an input vector. To ensure full compatibility with the notation used for K-Means, an RBF layer is defined using the same number of centers k , with parameters

$$\Theta = \{\mu_1, \dots, \mu_k\}, \quad \mu_j \in \mathbb{R}^d.$$

The response of the j -th unit is the scalar function

$$\text{RBF}_{\mu_j}(x) = \phi(\|x - \mu_j\|_2), \quad (6)$$

with Gaussian activation function that measures a normalized distance under some σ parameter

$$\phi(r) = \exp\left(-\frac{r^2}{2\sigma^2}\right). \quad (7)$$

To keep the original scalar notation $\text{RBF}_{\mu}(x)$ intact while making the k outputs explicit, the full RBF layer is expressed as the vector-valued map

$$\text{RBF}_{\Theta}(x) = \begin{bmatrix} \text{RBF}_{\mu_1}(x) \\ \vdots \\ \text{RBF}_{\mu_k}(x) \end{bmatrix} = \begin{bmatrix} \phi(\|x - \mu_1\|_2) \\ \vdots \\ \phi(\|x - \mu_k\|_2) \end{bmatrix} \in \mathbb{R}^k, \quad (8)$$

so each component corresponds exactly to the classical single-unit definition. The parameters μ_j are optimized via gradient-based learning like many NNs [Goodfellow, 2016].

In contrast with the closed-form centroid update in K-Means, the stochastic gradient descent yields the generic update rule

$$\mu'_j = \mu_j - \eta \nabla_{\mu_j} \mathcal{L}, \quad (9)$$

where \mathcal{L} denotes a differentiable objective functional whose explicit structure will be introduced in subsequent sections. At this stage, no particular form of \mathcal{L} is imposed; the analysis proceeds at the level of a general smooth loss in order to preserve compatibility with the variational constructions developed later.

Thus, in an RBF network the centers evolve continuously and may interact with deeper neural components under arbitrarily small gradient steps.

A key property of the Gaussian basis is the strict monotone correspondence between Euclidean distance and activation:

$$\|x_1 - \mu\| < \|x_2 - \mu\| \iff \exp(-\|x_1 - \mu\|^2) > \exp(-\|x_2 - \mu\|^2).$$

Therefore, the maximum-activation decision rule is equivalent to nearest-centroid assignment:

$$\arg \max_j \text{RBF}_{\mu_j}(x) = \arg \min_j \|x - \mu_j\|^2.$$

This induces the same Voronoi partition as K-Means,

$$S_i = \{x : i = \arg \min_j \|x - \mu_j\|^2\}.$$

3 Formal Comparison Between the K -Means Update and the RBF Update

In this section, we show the ways in which both models are the same under certain circumstances in the type of decision process under Γ -convergence and how the learning rate can be adapted to force a hard update in the process instead of gradient steps, serving as the backbone of this paper.

To analyze the limiting behavior of \mathcal{L}_σ as $\sigma \rightarrow 0$, we first approximate the K-Means distortion and converges to it in the sense of Γ -convergence, we analyze the limiting behavior of \mathcal{L}_σ as $\sigma \rightarrow 0$. and prove that each gradient step $\mu' \leftarrow \mu - \eta \nabla \mathcal{L}(\mu)$ is equivalent to $\mu_i = (1/|S_i|) \sum_{j \in S_i} x_j$ under certain circumstances.

3.1 Variational Reparametrization via Responsibilities

The classical K -Means distortion can be written as a joint optimization problem over centroids and assignment variables. Introducing binary indicators

$$r_{ij} \in \{0, 1\}, \quad \sum_{j=1}^k r_{ij} = 1 \quad \text{for all } i,$$

the distortion functional becomes

$$J(\mu) = \min_{r \in \mathcal{R}} \sum_{i=1}^n \sum_{j=1}^k r_{ij} \|x_i - \mu_j\|^2, \quad (10)$$

where

$$\mathcal{R} = \left\{ r \in \{0, 1\}^{n \times k} : \sum_{j=1}^k r_{ij} = 1 \right\}.$$

This formulation makes explicit that K -Means is an optimization problem over the product space

$$\mathcal{R} \times \mathbb{R}^{k \times d},$$

combining discrete assignments with continuous centroids.

The hard assignment rule

$$r_{ij} = \mathbf{1}_{\{j = \arg \min_\ell \|x_i - \mu_\ell\|^2\}}$$

is therefore the minimizer of (10) with respect to r for fixed μ . This variational formulation is the natural starting point for constructing continuous relaxations of the model.

3.2 Entropic Relaxation and Zero-Temperature Limit

A continuous relaxation of (10) is obtained by replacing the discrete set \mathcal{R} with the probability simplex

$$\Delta^{k-1} = \left\{ r_i \in \mathbb{R}^k : r_{ij} \geq 0, \sum_{j=1}^k r_{ij} = 1 \right\}.$$

For $\sigma > 0$, consider the entropically regularized functional

$$\mathcal{J}_\sigma(\mu, r) = \sum_{i=1}^n \sum_{j=1}^k r_{ij} \|x_i - \mu_j\|^2 + 2\sigma^2 \sum_{i=1}^n \sum_{j=1}^k r_{ij} \log r_{ij}. \quad (11)$$

For fixed μ , the minimizer of \mathcal{J}_σ with respect to r under the simplex constraint is given by

$$r_{ij}(\sigma; \mu) = \frac{\exp(-\|x_i - \mu_j\|^2/(2\sigma^2))}{\sum_{\ell=1}^k \exp(-\|x_i - \mu_\ell\|^2/(2\sigma^2))}. \quad (12)$$

Thus, the Softmax responsibilities arise as the exact minimizer of the entropically regularized distortion. Eliminating r yields the reduced functional

$$\mathcal{L}_\sigma(\mu) = \sum_{i=1}^n \sum_{j=1}^k r_{ij}(\sigma; \mu) \|x_i - \mu_j\|^2,$$

which coincides with the RBF-based objective previously introduced.

The parameter σ plays the role of temperature. As $\sigma \rightarrow 0$, the entropy term in (11) vanishes and the minimizer $r_{ij}(\sigma; \mu)$ concentrates on the set

$$A_i(\mu) = \arg \min_{1 \leq j \leq k} \|x_i - \mu_j\|^2.$$

Consequently,

$$r_{ij}(\sigma; \mu) \longrightarrow \mathbf{1}_{\{j \in A_i(\mu)\}},$$

and the entropically regularized model converges to the classical hard-assignment K -Means formulation.

Therefore, K -Means can be interpreted as the zero-temperature limit of an entropically relaxed clustering functional, and the RBF model arises as the continuous interior of this variational family.

3.3 Equivalence Between RBF Optimization and k -Means

To establish the equivalence between the optimal solutions of K -Means and those obtained by training an RBF network with an appropriate loss, we introduce the following construction. Let $\{x_i\}_{i=1}^n \subset \mathbb{R}^d$ be a dataset and let $\{\mu_j\}_{j=1}^k$ denote the trainable RBF centers. For $\sigma > 0$, define the soft assignment matrix by

$$r_{ij}(\sigma; \mu) = \frac{\exp(-\|x_i - \mu_j\|^2/(2\sigma^2))}{\sum_{\ell=1}^k \exp(-\|x_i - \mu_\ell\|^2/(2\sigma^2))}.$$

The RBF-network objective is then defined as the weighted distortion

$$\mathcal{L}_\sigma(\mu) = \sum_{i=1}^n \sum_{j=1}^k r_{ij}(\sigma; \mu) \|x_i - \mu_j\|^2. \quad (13)$$

This formulation mirrors the classical K -Means distortion, but with continuous responsibilities instead of hard assignments. The following result does not assert equivalence of the underlying models; rather, it establishes variational equivalence in the sense of Γ -convergence: as $\sigma \rightarrow 0$, the RBF objective \mathcal{L}_σ converges to the K -Means distortion J , and consequently their minimizers coincide in the limit.

Theorem 1 (Γ -limit and convergence of minimizers). *Let $X = \{x_i\}_{i=1}^n \subset \mathbb{R}^d$ be fixed and let $\mathcal{K} \subset \mathbb{R}^{k \times d}$ be compact. For $\sigma > 0$ define the soft clustering functional*

$$\mathcal{L}_\sigma(\mu) = \sum_{i=1}^n \sum_{j=1}^k r_{ij}(\sigma; \mu) \|x_i - \mu_j\|^2,$$

and the hard clustering functional

$$J(\mu) = \sum_{i=1}^n \min_{1 \leq j \leq k} \|x_i - \mu_j\|^2.$$

Then $\mathcal{L}_\sigma \xrightarrow{\Gamma} J$ on \mathcal{K} as $\sigma \rightarrow 0$. In particular, if $\sigma_m \rightarrow 0$ and $\mu^*(\sigma_m) \in \arg \min_{\mu \in \mathcal{K}} \mathcal{L}_{\sigma_m}(\mu)$, every accumulation point $\bar{\mu}$ of $\{\mu^*(\sigma_m)\}_m$ is a minimizer of J on \mathcal{K} .

Proof. Fix a sequence $\sigma_m \rightarrow 0$. We prove that $\mathcal{L}_{\sigma_m} \xrightarrow{\Gamma} J$ on \mathcal{K} .

Let $\mu_m \rightarrow \mu$ in \mathcal{K} . For each i and each m , the vector $r_{i \cdot}(\sigma_m; \mu_m)$ belongs to the probability simplex Δ^{k-1} and therefore defines a convex combination. Hence

$$\sum_{j=1}^k r_{ij}(\sigma_m; \mu_m) \|x_i - \mu_{m,j}\|^2 \geq \min_{1 \leq j \leq k} \|x_i - \mu_{m,j}\|^2.$$

Taking $\liminf_{m \rightarrow \infty}$ and using the continuity of $\mu \mapsto \min_j \|x_i - \mu_j\|^2$ (as a finite minimum of continuous functions), we obtain

$$\liminf_{m \rightarrow \infty} \sum_{j=1}^k r_{ij}(\sigma_m; \mu_m) \|x_i - \mu_{m,j}\|^2 \geq \min_{1 \leq j \leq k} \|x_i - \mu_j\|^2.$$

Summing over $i = 1, \dots, n$ yields

$$\liminf_{m \rightarrow \infty} \mathcal{L}_{\sigma_m}(\mu_m) \geq J(\mu),$$

which establishes the lim inf inequality.

To prove the lim sup inequality, fix $\mu \in \mathcal{K}$ and consider the constant sequence $\tilde{\mu}_m \equiv \mu$. For each i , as $\sigma_m \rightarrow 0$, the Softmax responsibilities concentrate on the set

$$A_i(\mu) := \arg \min_{1 \leq j \leq k} \|x_i - \mu_j\|^2,$$

while the weights assigned to its complement decay exponentially fast. Consequently,

$$\sum_{j=1}^k r_{ij}(\sigma_m; \mu) \|x_i - \mu_j\|^2 \longrightarrow \min_{1 \leq j \leq k} \|x_i - \mu_j\|^2.$$

Since the number of data points is finite, we may pass the limit inside the finite sum and conclude that

$$\lim_{m \rightarrow \infty} \mathcal{L}_{\sigma_m}(\tilde{\mu}_m) = J(\mu).$$

This proves the lim sup inequality and therefore $\mathcal{L}_{\sigma_m} \xrightarrow{\Gamma} J$ on \mathcal{K} .

Finally, since \mathcal{K} is compact, every sequence of minimizers $\mu^*(\sigma_m)$ admits accumulation points. Compactness also guarantees equi-coercivity. By the fundamental theorem of Γ -convergence (see [Dal Maso, 2012], *An Introduction to Γ -Convergence*), every accumulation point of minimizers of \mathcal{L}_{σ_m} is a minimizer of J on \mathcal{K} . \square

The previous result shows that, in the vanishing-temperature regime, the optimal RBF centers converge to the optimal K-Means centroids. This convergence is not specific to the Softmax-based responsibilities in Eq. 12, but extends to alternative assignment mechanisms, including entropic and sparse mappings such as Entmax-1.5, whose validity will be established later in Section 3.6.

The previous theorem extends to the unconstrained case under a coercivity assumption on J .

Corollary 1. *Assume that J is coercive on $\mathbb{R}^{k \times d}$. Then the conclusion of Theorem 1 remains valid with $\mathcal{K} = \mathbb{R}^{k \times d}$.*

The proof is given in Appendix A.1.

3.4 Updating Process Equivalence

A central objective of our analysis is to show that the neural formulation inherits the fixed points of classical K-Means. To make this explicit, we isolate the centroid-update mechanism and study it under fixed responsibilities $r_{ij}(\sigma)$ and validate that, under certain circumstances, the update process is equivalent. This decouples the optimization of the centers from the nonlinear dependence induced by the assignment rule and reveals the underlying structure: a weighted least-squares problem whose minimizer corresponds to the soft centroid, and whose hard limit recovers the standard K-Means update.

For fixed responsibilities, the loss reduces to the weighted quadratic form

$$\mathcal{L}_\sigma(\mu) = \sum_{j=1}^k \sum_{i=1}^n r_{ij}(\sigma) \|x_i - \mu_j\|^2,$$

which coincides with a mean-squared error objective with weights $r_{ij}(\sigma)$. Differentiating with respect to μ_j yields

$$\nabla_{\mu_j} \mathcal{L}_\sigma = 2 \left(\sum_i r_{ij}(\sigma) \right) \mu_j - 2 \sum_i r_{ij}(\sigma) x_i,$$

a linear expression of the form $a_j \mu_j - b_j$ which proves that the models have a similar solution.

Lemma 1 (Soft centroid as fixed point). *For fixed responsibilities $r_{ij}(\sigma)$, the gradient descent update*

$$\mu'_j = \mu_j - \eta \nabla_{\mu_j} \mathcal{L}_\sigma$$

converges, for $\eta a_j < 1$, to the unique update process

$$\mu_j^* = \frac{\sum_i r_{ij}(\sigma) x_i}{\sum_i r_{ij}(\sigma)}.$$

Proof. With $a_j = \sum_i r_{ij}(\sigma)$ and $b_j = \sum_i r_{ij}(\sigma) x_i$, the gradient update takes the affine form

$$\mu'_j = (1 - \eta a_j) \mu_j + \eta b_j.$$

For $\eta a_j < 1$, this iteration is a contraction and converges to its unique fixed point $\mu_j^* = b_j / a_j$, which yields the stated expression. \square

Remark (Step size and contractive dynamics). The condition $\eta a_j < 1$ ensures that the affine update

$$\mu'_j = (1 - \eta a_j) \mu_j + \eta b_j$$

is a contraction toward its unique fixed point. Choosing

$$\eta = \frac{1}{2a_j} = \frac{1}{2 \sum_i r_{ij}(\sigma)}$$

not only satisfies the contraction condition but yields

$$\mu'_j = \frac{b_j}{a_j},$$

so that convergence occurs in a single step. In the hard-assignment regime, where $a_j \rightarrow |S_j|$, this reduces to $\eta = (2|S_j|)^{-1}$, which is precisely the learning rate appearing in Theorem 2. Hence, the classical K-Means update is the specific contractive choice of step size in the limiting discrete setting. Moreover, in the practical implementation (Algorithm 2), the discrete term $|S_j|$ is replaced by its differentiable counterpart $r_j = \sum_i R_{ij}$, which provides a smooth approximation of the point count and enables gradient flow toward the cluster centers.

In the vanishing-temperature regime $\sigma \rightarrow 0$, the responsibilities collapse to hard assignments and Lemma 1 reduces to the classical K-Means centroid.

When the dependence of $r_{ij}(\sigma)$ on the parameters is restored as in Softmax or Entmax-based assignments, additional terms appear in the gradient, recovering the neural-network update studied earlier. In the hard-assignment limit, these terms vanish and the update coincides exactly with K-Means as a method.

Theorem 2 (K-Means update as a gradient step). *Let S_j denote the cluster associated with centroid μ_j , and consider the loss*

$$L(\{\mu_j\}) = \sum_{j=1}^k \sum_{x \in S_j} \|x - \mu_j\|^2.$$

Then the gradient descent update $\mu'_j = \mu_j - \eta \nabla_{\mu_j} L$ coincides with the classical K-Means update

$$\mu_j^{\text{KM}} = \frac{1}{|S_j|} \sum_{x \in S_j} x$$

for the choice $\eta = (2|S_j|)^{-1}$.

Proof. The gradient of the expansion of the Eq. 13 with respect to the parameters μ_j is given by

$$\nabla_{\mu_j} L = 2|S_j|\mu_j - 2 \sum_{x \in S_j} x.$$

which substituting into the gradient step Eq. 9 and rearranging and factorizing μ_j the terms yields to

$$\mu'_j = (1 - 2\eta|S_j|)\mu_j + 2\eta \sum_{x \in S_j} x.$$

Choosing $\eta = (2|S_j|)^{-1}$ annihilates the dependence on μ_j and gives $\mu'_j = \mu_j^{\text{KM}}$, as claimed. \square

Remark on Gradient Consistency: Although the responsibilities $r_{ij}(\mu)$ in Eq. 12 depend on the centroids, the total gradient $\nabla_{\mu_j} L_\sigma$ simplifies in the vanishing-temperature regime. As $\sigma \rightarrow 0$, r_{ij} converges to a piecewise constant indicator function $1_{\{i \in S_j\}}$, whose derivative is zero almost everywhere. Furthermore, the exponential decay shown in Theorem 3 ensures that these additional terms vanish faster than the growth of the distance components, recovering the exact K-Means update rule.

In this way, discretizations can be avoided by choosing the correct values of the learning rate η with respect to the size $|S_j|$, which is a discrete term that can be approximated by the sum $|S_j| \approx \sum_{i=1}^n r_{ij}(\sigma)$ and converge when $\sigma \rightarrow 0$ converges to $\sum_{i=1}^n r_{ij} \xrightarrow{\sigma \rightarrow 0} |S_j|$.

These approximations lead to an unsupervised regularization term as a loss function, which coincides with the scope of K-Means.

3.5 Mean Error Between RBF—Soft Clustering and K-Means

We now quantify the rate at which the soft RBF centroids converge to the hard K-Means centroids as the temperature σ vanishes. Under a uniform cluster-separation assumption, the deviation decays exponentially at $1/\sigma^2$, a rate strictly stronger than any polynomial convergence. This assumption serves a dual role: it clarifies the regime in which the two methods are provably equivalent, and it provides a theoretical baseline against which empirical convergence can be assessed in the experimental sections.

Theorem 3 (Exponential Convergence of RBF Centroids). *Let $X = \{x_i\}_{i=1}^n \subset \mathbb{R}^d$ with $\|x_i\| \leq R$, and let $\{\mu_j^{\text{KM}}\}_{j=1}^k$ be the K-Means centroids inducing Voronoi cells $\{S_j\}_{j=1}^k$ with $|S_j| \geq \alpha n$ for some $\alpha > 0$. Define the soft responsibilities*

$$r_{ij}(\sigma) = \frac{\exp(-\|x_i - \mu_j\|^2 / (2\sigma^2))}{\sum_{\ell=1}^k \exp(-\|x_i - \mu_\ell\|^2 / (2\sigma^2))}$$

and the associated soft centroids

$$\tilde{\mu}_j(\sigma) = \frac{\sum_{i=1}^n r_{ij}(\sigma) x_i}{\sum_{i=1}^n r_{ij}(\sigma)}.$$

Let $d_{i,(1)}$ and $d_{i,(2)}$ denote the smallest and second-smallest distances from x_i to the centroids, and define the margin $\gamma_i = d_{i,(2)} - d_{i,(1)}$ with $\gamma_{\min} = \min_i \gamma_i > 0$. Then, for all σ sufficiently small,

$$\|\tilde{\mu}_j(\sigma) - \mu_j^{\text{KM}}\| \leq \frac{2R}{\alpha} (k-1) \exp\left(-\frac{\gamma_{\min}^2}{2\sigma^2}\right).$$

Proof. Fixing a data point x_i and let j_i denote the index of its nearest centroid. For any $\ell \neq j_i$,

$$\|x_i - \mu_\ell\|^2 - \|x_i - \mu_{j_i}\|^2 = (d_{i,(2)} - d_{i,(1)})(d_{i,(2)} + d_{i,(1)}) \geq \gamma_i^2,$$

which implies

$$\exp\left(-\frac{\|x_i - \mu_\ell\|^2 - \|x_i - \mu_{j_i}\|^2}{2\sigma^2}\right) \leq e^{-\gamma_i^2/(2\sigma^2)}.$$

If $i \in S_j$, this yields $1 - r_{ij} \leq (k-1)e^{-\gamma_i^2/(2\sigma^2)}$, while for $i \notin S_j$ we directly obtain $r_{ij} \leq (k-1)e^{-\gamma_i^2/(2\sigma^2)}$. Hence, uniformly in i and j ,

$$|r_{ij} - \mathbf{1}_{\{i \in S_j\}}| \leq (k-1)e^{-\gamma_{\min}^2/(2\sigma^2)}.$$

Using this estimate and $\|x_i\| \leq R$, the centroid deviation satisfies

$$\|\tilde{\mu}_j(\sigma) - \mu_j^{\text{KM}}\| \leq \frac{R \sum_i |r_{ij} - \mathbf{1}_{\{i \in S_j\}}|}{\sum_{i \in S_j} r_{ij}}.$$

For σ small enough, the denominator is bounded below by $\sum_{i \in S_j} r_{ij} \geq |S_j|/2 \geq \alpha n/2$, yielding

$$\|\tilde{\mu}_j(\sigma) - \mu_j^{\text{KM}}\| \leq \frac{2R}{\alpha}(k-1)e^{-\gamma_{\min}^2/(2\sigma^2)}.$$

□

This result clarifies the geometric origin of the exponential convergence. The approximation error is controlled by the minimal separation margin γ_{\min} , which measures how decisively most points are assigned to a single Voronoi cell. When most of the data lies well inside their clusters, the soft responsibilities concentrate exponentially fast, forcing the soft centroids to align with the hard K -Means centroids. Consequently, the convergence rate cannot exceed what is imposed by the typical inter-cluster separation, and vanishing margins necessarily degrade the approximation.

The boundedness assumption $\|x_i\| \leq R$ is equally essential. It prevents the centroid deviation from being dominated by a small number of distant points with non-negligible soft weights. In non-compact settings or for heavy-tailed distributions, this control is lost and the centroid error may diverge even when the responsibilities converge pointwise.

3.6 Computational Problems Along the Decision Process: Softmax Instability and the Entmax-1.5 Solution

The continuous assignment mechanism introduced in Eq. (13) relies on a Softmax transformation applied to the negative squared distances. Although this choice is mathematically consistent and yields a smooth relaxation of the K -Means assignments together with a strong convergence rate, it becomes numerically unstable in the regime relevant for recovering hard partitions. Specifically, when $\sigma \rightarrow 0$, the RBF activations

$$\exp\left(-\frac{\|x_i - \mu_j\|^2}{2\sigma^2}\right)$$

become increasingly peaked and rapidly underflow to zero in finite-precision arithmetic. For instance, with a distance of 3 and $\sigma = 0.01$, the exponent evaluates to $\exp(-900)$, far below standard floating-point resolution. In this limit, the Softmax saturates, gradients collapse, and the model becomes unable to propagate meaningful updates. A mismatch therefore arises between the theoretical limit $r_{ij}(\sigma) \rightarrow r_{ij}$ and its numerical evaluation, preventing convergence to the exact K -Means solution even though the functional \mathcal{L}_σ remains well-defined.

To address this issue, we replace Softmax with the Entmax-1.5 transformation introduced in [Peters et al., 2019], defined as the optimizer of a Tsallis-regularized prediction problem. Entmax-1.5 produces sparse probability vectors, maintains differentiability, and grows polynomially rather than exponentially with respect to the logits. For an input vector $z \in \mathbb{R}^k$, the mapping satisfies

$$\text{Entmax}_{1.5}(z)_j = \left[\frac{1}{2}(z_j - \tau(z)) \right]_+^2,$$

where $\tau(z)$ enforces normalization. In contrast with Softmax, Entmax distributes mass over a subset of entries and suppresses excessively large activations. Consequently, even when σ is small and the values $-\|x_i - \mu_j\|^2/(2\sigma^2)$ diverge, the induced probabilities remain numerically controlled.

This modification preserves the theoretical framework for two reasons. First, Entmax-1.5 retains the ordering structure of the activations and therefore yields assignments consistent with the same Voronoi decision regions as $\sigma \rightarrow 0$. Second,

although Shannon entropy is replaced by a Tsallis-type regularization, the variational structure is maintained and the responsibilities converge to hard cluster indicators in the zero-temperature limit due to polynomial sparsity.

We now formalize the convergence behavior of the induced centroids under Entmax–1.5 and show that the hard K -Means solution is still recovered in the zero-temperature regime, albeit at a polynomial rate.

Theorem 4 (Centroid Deviation for Entmax–1.5). *Let $X = \{x_i\}_{i=1}^n \subset \mathbb{R}^d$ with $\|x_i\| \leq R$, and let $\{\mu_j^{\text{KM}}\}_{j=1}^k$ induce Voronoi cells $\{S_j\}_{j=1}^k$ satisfying $|S_j| \geq \alpha n$ for some $\alpha > 0$. Define the Entmax–1.5 responsibilities*

$$r_{ij}(\sigma) = \text{Entmax}_{1.5} \left(-\frac{\|x_i - \mu_j\|^2}{2\sigma^2} \right), \quad \tilde{\mu}_j(\sigma) = \frac{\sum_{i=1}^n r_{ij}(\sigma) x_i}{\sum_{i=1}^n r_{ij}(\sigma)}.$$

Let $\gamma_i = d_{i,(2)} - d_{i,(1)}$ and assume $\gamma_{\min} = \min_i \gamma_i > 0$. Then there exists a constant $C = C(R, k, \alpha, \gamma_{\min}) > 0$ such that, for all sufficiently small σ ,

$$\|\tilde{\mu}_j(\sigma) - \mu_j^{\text{KM}}\| \leq C \sigma.$$

Proof. Entmax–1.5 is Lipschitz continuous with respect to its input vector. Writing $z_{ij} = -\|x_i - \mu_j\|^2 / (2\sigma^2)$, the gap between the largest and second largest components satisfies

$$z_{i,(1)} - z_{i,(2)} = \frac{\gamma_i^2}{2\sigma^2}.$$

By Lipschitz continuity, this implies the lower bound

$$|r_{ij}(\sigma) - \mathbf{1}_{\{i \in S_j\}}| \leq C_1 \frac{\sigma}{\gamma_{\min}},$$

for a constant C_1 depending only on k . Using $\|x_i\| \leq R$ and the lower bound $\sum_{i \in S_j} r_{ij}(\sigma) \geq \alpha n / 2$ for small σ enough, we obtain

$$\|\tilde{\mu}_j(\sigma) - \mu_j^{\text{KM}}\| \leq C \sigma,$$

where C depends on R, k, α , and γ_{\min} . □

This result confirms that Entmax–1.5 preserves convergence toward the K -Means centroids as $\sigma \rightarrow 0$, though at an algebraic rate $O(\sigma)$ instead of the exponential rate observed under Softmax-based RBF clustering. The empirical rate measurements reported in Section 4.3 are consistent with this bound. While Gaussian activations provide analytical convenience, Entmax–1.5 offers a numerically stable alternative without altering the limiting solution.

4 Experimental Testing

This section evaluates the empirical correspondence between classical K -Means and the soft-RBF formulation derived in the previous sections. Our primary objective is to measure how closely the soft-assignment centroids track the hard K -Means fixed point as the temperature parameter σ decreases, thereby testing the theoretical convergence assertions established earlier. We further assess a stabilized variant that replaces the Softmax-based responsibilities with Entmax-1.5, ensuring well-behaved gradients in the low-temperature regime.¹

4.1 Evaluation Setting

Convergence Measure. To quantify how the soft-RBF centroids approach the hard K -Means solution, we compare centroid configurations under the deviation

$$d(\mu, \mu') = \sum_{j=1}^k \|\mu_j - \mu'_j\|, \quad \mu, \mu' \in \mathbb{R}^{k \times d}.$$

For a fixed initialization μ_0 , let $\mu_0^{(\text{KM})}$ denote the K -Means solution obtained from that seed, and let $\mu_0^{(\text{soft})}(\sigma)$ denote the corresponding soft-RBF solution at temperature σ . The expected discrepancy at scale σ is

$$R_{\mu_0}(\sigma) = \mathbb{E} \left[d \left(\mu_0^{(\text{KM})}, \mu_0^{(\text{soft})}(\sigma) \right) \right],$$

¹All algorithms and implementations will be publicly available at <https://github.com/FelixStaff/KmeansAsRBF>.

where the expectation is taken over all randomness in the optimization dynamics of the soft-RBF update rule.

Empirically, the mapping $\sigma \mapsto R_{\mu_0}(\sigma)$ is evaluated on a discrete grid $\{\sigma_1, \dots, \sigma_L\}$, producing

$$\widehat{R} = \{R_{\mu_0}(\sigma_1), \dots, R_{\mu_0}(\sigma_L)\}.$$

This curve measures how the continuous soft-centroid dynamics collapse toward the discrete K-Means fixed point when the initialization is fixed.

Fixed vs. Resampled Initialization. Two complementary evaluation protocols are used, differing in how initializations enter the computation of the discrepancy metric:

1. *Fixed initialization protocol.* A single pool of M initial centroid configurations is generated once and reused across all σ values. The resulting metric, denoted $R_{\text{fixed}}(\sigma)$, isolates the effect of the temperature parameter by holding initialization variability constant. The complete evaluation procedure is given in Algorithm 3.

2. *Resampled initialization protocol.* For every temperature value σ_ℓ , fresh initializations are drawn independently. The corresponding metric, denoted $R_{\text{resampled}}(\sigma)$, reflects both the smoothing effect of the soft assignment and the variability induced by random seeding. The procedure is shown in Algorithm 4.

These two metrics capture different aspects of convergence. $R_{\text{fixed}}(\sigma)$ exposes how the soft-RBF dynamics alone deform the centroid trajectories for a fixed seed, while $R_{\text{resampled}}(\sigma)$ provides an initialization-averaged view of the landscape and quantifies robustness across multiple random seeds.

Initialization-Averaged Convergence. When averaging over multiple seeds generated in the list $\{\mu_0^{(1)}, \dots, \mu_0^{(M)}\}$, the global convergence profile becomes

$$\bar{R}(\sigma) = \frac{1}{M} \sum_{m=1}^M R_{\mu_0^{(m)}}(\sigma),$$

which summarizes the expected proximity between the soft-RBF solution and the K-Means fixed point across the entire initialization distribution.

4.1.1 Sigma-Value Sampling and Rate-of-Convergence Fit

The experimental setting is governed by three parameters: the number of clusters k , the number of optimization steps T , and the temperature σ . Because the RBF-based responsibilities scale exponentially in $1/\sigma$, while Entmax-1.5 exhibits a first-order polynomial scaling $O(\sigma)$ near zero, a linear schedule for σ leads to degenerate behavior as $\sigma \rightarrow 0$. To sample the dynamics uniformly across scales, we adopt a logarithmic schedule:

$$\sigma_t = \sigma_{\min} \left(\frac{\sigma_{\max}}{\sigma_{\min}} \right)^{\frac{t}{L-1}}, \quad \sigma_{\min} = 10^{-3}, \quad \sigma_{\max} = 10^{-1}, \quad L = 50.$$

For each σ_t , we measure the centroid deviation

$$d_j(\sigma_t) = \|\mu_j^{(\text{KM})} - \mu_{\pi(j)}^{(\text{soft})}(\sigma_t)\|,$$

where π denotes the optimal permutation aligning the two centroid sets. The aggregated statistic $R(\sigma_t)$ combines these deviations and quantifies how the soft-RBF centroids collapse toward the K-Means fixed point as σ decreases.

To quantify the empirical exponent governing this collapse, we perform a log-log linear fit. Define

$$x_\ell = \log \sigma_\ell, \quad y_\ell = \log R(\sigma_\ell),$$

so that the model

$$y_\ell \approx m x_\ell + b$$

corresponds exactly to the power-law decay $R(\sigma) \approx C \sigma^m$ with $C = e^b$.

This regression isolates the slope m , which acts as an effective complexity exponent. Beyond a scaling coefficient, m captures the empirical rate at which the soft assignments harden and the induced Voronoi partitions stabilize as $\sigma \downarrow 0$. Within our framework, this exponent provides a direct experimental validation of the convergence theorems.

For standard RBF (Softmax), Theorem 3 establishes exponential convergence toward the hard assignment regime. Since exponential decay does not admit a finite polynomial exponent in a log-log regression, the fitted slope m is expected to increase in magnitude as $\sigma \rightarrow 0$, reflecting super-polynomial contraction.

For Entmax-1.5, Theorem 4 proves a polynomial convergence rate of order $O(\sigma)$. Consequently, the fitted exponent m should stabilize near 1, consistent with first-order polynomial decay.

Therefore, both the magnitude and stability of m provide a measurable bridge between the theoretical convergence bounds and the observed optimization behavior, linking the sampling strategy in σ with the empirical rate at which the soft-centroid dynamics approximate the hard K-Means solution.

4.1.2 Algorithmic Considerations

To ensure an unbiased comparison, both algorithms are implemented in their full, uncompromised form. For K-Means, we use the standard assignment–update loop without heuristics or acceleration; the exact procedure is listed in Algorithm 1. For the RBF network, we implement the complete gradient update, including the derivatives of the responsibilities with respect to the centers and widths. This avoids the common EM-style shortcuts and ensures that the dynamics match the theoretical formulation developed earlier. The full update is shown in Algorithm 2.

For the evaluation stage, reconstruction error and assignment stability are computed explicitly at each iteration using the routines in Algorithms 3 and 4. These procedures quantify how both models evolve and allow a direct, iteration-level comparison of their trajectories.

4.2 Benchmark on Synthetic Geometries

We evaluate the soft-to-hard centroid convergence across four synthetic datasets designed to span distinct geometric regimes: Euclidean separation, nonlinear manifolds, polar distortions, and radial structures. This diversity ensures that convergence is not restricted to a particular topology.

Dataset	Geometric Regime	Parameters
Gaussian Blobs	Well-separated Euclidean clusters	centers = 3
Two Moons	Nonlinear manifold	noise = 0.05
Spiral	Nonconvex polar structure	radius = 3
Circles	Radial separation	factor = 0.5, noise = 0.05

Table 1: Synthetic datasets used to evaluate soft-to-hard centroid convergence.

All experiments were conducted with $k = 3$ clusters over $T = 150$ training steps. For statistical robustness, each configuration was repeated over $M = 200$ independent runs.

4.3 Convergence Rate Results

We report the centroid–discrepancy curves $R(\sigma)$ across the full logarithmic temperature schedule. For every dataset and every value of σ , the soft-RBF centroids collapse monotonically toward the hard K-Means solution, producing strictly decreasing error profiles as temperature shrinks. This behaviour holds across all geometries, including Gaussian blobs, nonlinear manifolds, spirals, and concentric structures.

To quantify the rate of convergence, we fit a linear model on the log-log relation between error and temperature defined in the Section 4.1.1,

$$\log R(\sigma) = m \log \sigma + b.$$

The slope m estimates the exponent in the asymptotic law $R(\sigma) = O(\sigma^m)$. With standard RBF responsibilities, the estimated rate matches the decay previously proven. Under the Entmax-1.5 transformation, however, the empirical exponent consistently stabilizes around $m \approx 1$ indicating a linear-type decay, consistent with the almost piecewise-linear nature of Entmax–1.5 assignments at low temperature and empirically verify that $m > 1$ across all test cases.

Figure 1b summarizes the estimated exponents across datasets. All fitted values satisfy $m > 1$, confirming a faster-than-linear decay and remaining strictly below the theoretical upper bound of Theorem 4. The only deviation appears in the Gaussian blobs configuration shown in Fig. 1a. This anomaly arises from the dataset-dependent constants R and γ_{\min} , which cap the maximum attainable discrepancy: since centroid initialization is fixed, these constants remain unchanged throughout the schedule and impose an upper limit on $R(\sigma)$ for large σ . This saturates the curve and distorts the slope estimation. We keep this initialization to avoid cherry-picking and to illustrate the behaviour under controlled centroid positions, even if it induces this dataset-specific saturation effect.

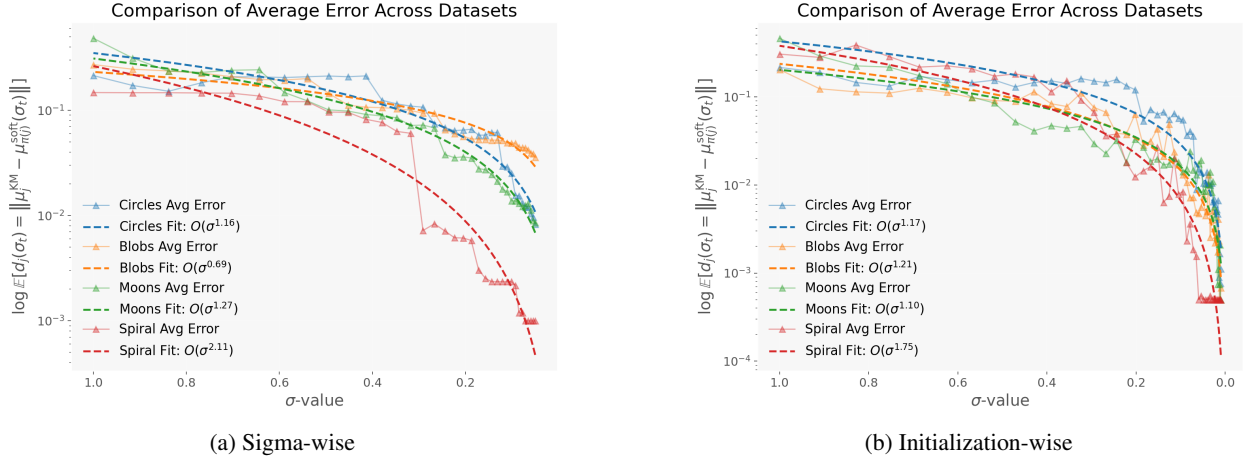


Figure 1: Centroid discrepancies $d_j(\sigma)$ under two temperature–decay protocols. (*Sigma-wise*) A fixed centroid initialization is evaluated across a decreasing σ schedule, measuring the deviation from the hard K-Means solution at each temperature. (*Initialization-wise*) Centroids are re-initialized independently over M runs, and the discrepancy is averaged across initializations for each σ . In both settings, all datasets exhibit a monotone collapse of soft-RBF centroids toward the K-Means centroids as $\sigma \rightarrow 0$.

4.4 Qualitative Behaviour

The qualitative behaviour of the smoothed model aligns tightly with the theoretical predictions. As σ decreases, the centroid trajectories collapse onto the classical K-Means fixed points, producing visually indistinguishable partitions once the temperature enters the low- σ regime. In well-separated datasets such as Gaussian blobs, the collapse is immediate and stable, with smooth paths that converge almost radially toward the hard solution, reflecting the isotropic geometry of the data.

For nonlinear geometries such as moons, spirals, and concentric circles, the trajectories display more irregular and winding paths. While isotropic datasets exhibit near-radial convergence, non-convex manifolds induce sharper directional changes along the optimization path. This behaviour highlights the soft-to-hard transition of the attraction basins: at higher temperatures, a centroid is influenced by a diffuse, global average of the dataset, whereas as $\sigma \rightarrow 0$, the responsibility mass concentrates rapidly, forcing the centroid to re-align with its emerging Voronoi cell. In complex geometries, this realignment often produces abrupt turns as the trajectory adapts to the underlying manifold structure.

The centroid-path visualizations in Figure 2 illustrate this phenomenon: each trajectory contracts toward a single starred point corresponding to the K-Means optimum, confirming that the qualitative dynamics of the smoothed system reproduce the hard clustering geometry in the limit $\sigma \rightarrow 0$.

5 Extensions and Discussion

Besides the theoretical contribution, the proposed reparametrization yields a fully differentiable and continuous representation of the K-Means objective that can be used in deep learning problems. To apply everything, we can model a loss function. Let $r_{ij}(\theta)$ denote the differentiable assignment mechanism (e.g., the RBF–Entmax–1.5 construction of Section 3.6 [Peters et al., 2019]) and let $\mu = (\mu_1, \dots, \mu_k)$ be the trainable centroids. The centroid loss

$$\mathcal{L}_{\text{kmeans}}(\theta, \mu) = \sum_{j=1}^k \sum_{i=1}^n r_{ij}(\theta) \|x_i - \mu_j\|^2$$

is smooth in all parameters, which enables direct incorporation into any neural architecture. In particular, models such as [Zhu et al., 2011, Faraoun and Boukelif, 2006, Caron et al., 2018], which traditionally embed K-Means heuristically or as a postprocessing stage, can instead integrate the clustering dynamics by optimizing (ϕ, μ) jointly inside the main problem modeling.

This makes it possible to embed K-Means inside arbitrary architectures by augmenting the objective with the addition of a regularization term

$$\min_{\phi, \mu} \mathcal{L}_{\text{task}}(\phi) + \lambda \mathcal{L}_{\text{kmeans}}(\phi, \mu).$$

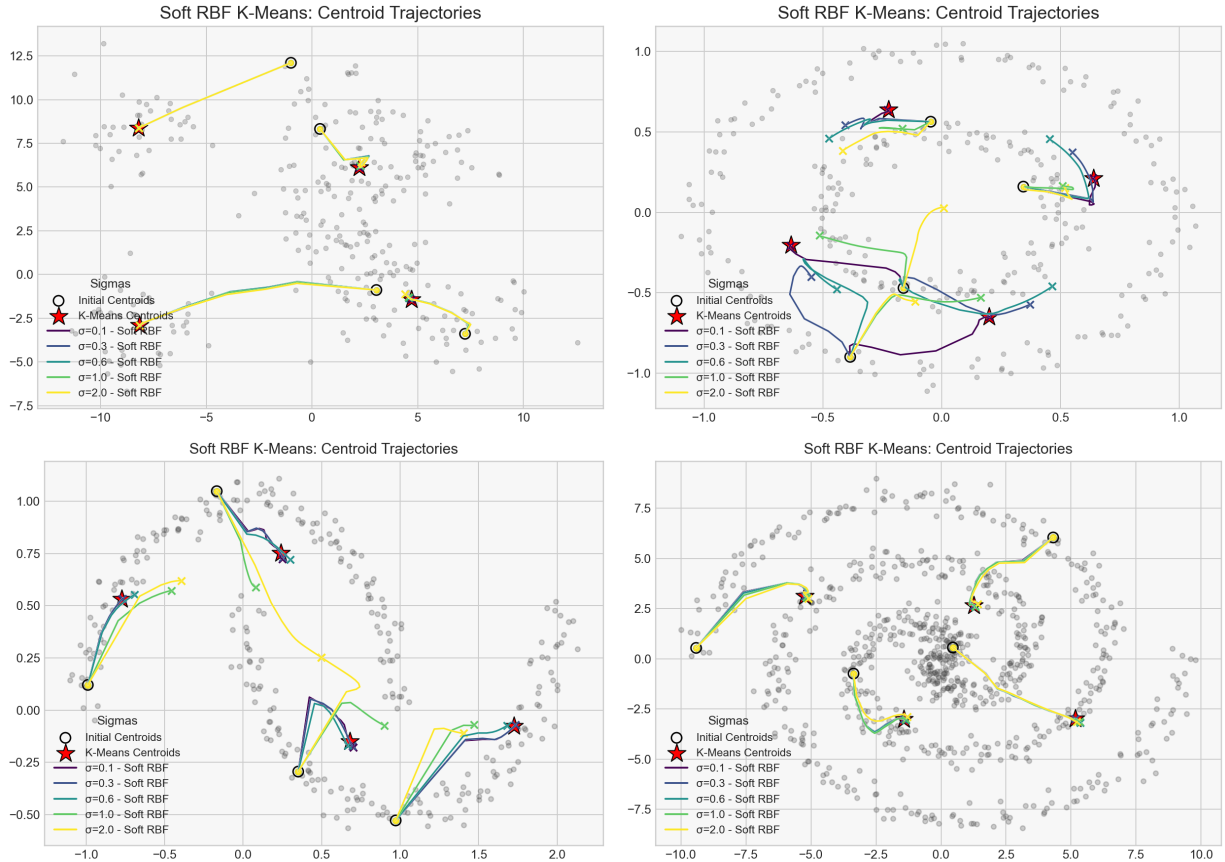


Figure 2: Convergence paths of the smoothed centroids as σ decreases. Each curve shows the trajectory from initialization to its final position. As $\sigma \rightarrow 0$, all paths collapse onto the starred point, which corresponds to the true K-Means solution, demonstrating that the smoothed formulation converges to the hard K-Means optimum.

The gradient

$$\nabla_{\mu} \mathcal{L}_{\text{kmeans}} = 2 \sum_{i=1}^n r_{ij}(\theta) (\mu_j - z_i)$$

updates the centroids continuously at each iteration, while $\nabla_{\phi} \mathcal{L}_{\text{kmeans}}$ imposes smooth cluster separation directly in the latent space. This removes the need for alternating minimization or external recomputation of K-Means and synchronizes centroid dynamics with the evolution of the representation learned by the network.

Some remark concerns geometric expressiveness. The differentiable formulation does not extend the representational capacity of K-Means: the method remains confined to Euclidean Voronoi partitions and is inadequate for nonlinear or manifold-structured data [Hastie et al., 2005, Dhillon et al., 2004]. Its contribution is computational rather than geometric. The reparametrization provides a stable, differentiable surrogate that enables embedding K-Means inside neural networks, but applications requiring nonlinear cluster geometry must still rely on richer clustering objectives or manifold-aware distances.

5.1 High Dependency on the Shape of the Data

The results in Figure 1 show that the convergence rates differ markedly across datasets, with large deviations in the values of m . In isotropic datasets such as Blobs and Circles, convergence is consistently stable, as their geometry naturally favors the soft-to-hard transition of the algorithm. In contrast, datasets with more complex manifolds, such as Moons and Spirals, exhibit significantly faster yet more irregular convergence patterns.

This disparity is a direct consequence of the geometry-dependent loss landscape. In Gaussian Blobs, the gradient flow remains stable because clusters are separated by clear Euclidean margins, producing well-defined attraction basins. However, in manifold-structured data such as Moons, these attraction regions become highly sensitive to

the temperature parameter. As σ decreases and responsibilities sharpen, the gradient dynamics shift from global data-averaging toward localized centroid estimation. The observed irregularity therefore reflects a deformation of local minima: small variations in σ can substantially alter the effective ownership of points between neighboring clusters, increasing path-dependency in non-convex regimes despite the theoretical equivalence of the formulations.

When plotting the centroid trajectories as in Figure 2, some datasets still display relatively coherent paths: even under large values of σ , certain initializations lead to similar convergence behavior. However, other initial points reveal strong divergence as σ varies, while a subset of trajectories shows a smoother, almost differential evolution, where the centroids slide progressively as σ decreases.

5.2 Deep RBF Models Exploration

A natural question is how these behaviors change once deep NN are introduced. In practice, this setting is equivalent to running K-Means on the latent space of a pre-trained network, as commonly done in several applications [Gao et al., 2020, Caron et al., 2018]. The central issue is how to shape the network’s training so that its latent manifold becomes genuinely useful for clustering.

As discussed at the beginning of Section 5, combining multiple loss terms can force the network to mold its internal manifold [Belghazi et al., 2018]. However, such constraints often push the latent space toward almost isotropic structures, thereby suppressing richer geometric features such as curvature, convexity, and general nonlinear patterns that can be recovered under the addition of a nonlinear loss function [de Jesús Félix Arredondo et al., 2025]. K-Means limits the capacity of the model to capture complex variations in the data.

For this reason, and consistent with the evidence reported in [Gao et al., 2023], we discourage the use of K-Means when the underlying task involves highly nonlinear manifolds or intricate convex structures. Forcing the latent space toward isotropy ultimately erodes the very geometric properties that deep models are supposed to exploit.

Despite these geometric constraints, the practical adoption of the SoftRBF framework within deep learning pipelines depends not only on its representational limits but also on its operational feasibility. While the previous discussion cautions against its use in highly non-linear manifolds, the transition from a discrete algorithm to a differentiable one must remain computationally viable. This leads to a critical examination of whether the benefits of gradient-based optimization and end-to-end integration come at a significant cost in terms of efficiency.

5.3 Computational Efficiency and Practical Trade-offs

The differentiable formulation and the classical K-Means share the same structural bottleneck: evaluating all pairwise distances. The main difference lies in how assignments are produced. Classical K-Means uses a hard $\arg \min$ step, while the SoftRBF-Net replaces it with an Entmax-1.5 projection, introducing an additional sorting cost. Thus, the choice between the two methods depends on whether the benefits of differentiability and sparsity compensate for this small overhead.

Let $D \in \mathbb{R}^{n \times d}$ be the dataset, with k clusters and T outer iterations.

K-Means Each iteration computes all distances $D_{ij} = \|x_i - \mu_j\|^2$, assigns each point via $S_i = \arg \min_j D_{ij}$, and recomputes the centroids. The distance evaluation dominates the computation:

$$C_{\text{KMeans}} = \Theta(nkd), \quad \text{Time}(\text{K-Means}) = \Theta(Tnk d).$$

Memory usage is $O(nd + nk)$.

SoftRBF-Net SoftRBF-Net performs the same distance evaluations, followed by the Entmax-1.5 projection, which adds an $O(k \log k)$ sorting step per sample. Accumulating sufficient statistics remains $O(nkd)$:

$$C_{\text{SoftRBF}} = \Theta(nk(d + \log k)), \quad \text{Time}(\text{SoftRBF}) = \Theta(Tnk(d + \log k)).$$

When Entmax-1.5 produces sparse assignments with expected sparsity $s \ll k$, the accumulation step reduces to $O(nsd)$, often yielding lower empirical cost than classical K-Means.

The differentiable formulation introduces only a modest $O(k \log k)$ computational overhead relative to classical K-Means. This cost becomes negligible once sparsity emerges in the assignment vectors, making SoftRBF networks attractive in settings where gradient-based optimization, end-to-end training, or structured sparsity provide practical advantages.

In full deep learning pipelines, however, each update entails redundant gradient computations that are unnecessary in the purely combinatorial K-Means algorithm. Moreover, the use of Entmax-1.5 is not mandatory: alternative stable

activation functions can be employed to induce sparsity while preserving the same limiting behaviour and theoretical equivalence.

6 Conclusions

This work provides a rigorous correspondence between classical K-Means and a differentiable RBF formulation based on smooth responsibilities. The loss \mathcal{L}_σ converges to the standard distortion as $\sigma \rightarrow 0$, and the centroid dynamics arise as continuous relaxations of the discrete update. This yields a stable gradient-based mechanism in which centroids and latent representations can be optimized jointly inside a neural architecture.

The proposed framework enables end-to-end integration of clustering by simply augmenting the task loss with a differentiable centroid term, avoiding alternating procedures and eliminating the need to recompute K-Means externally. The use of Entmax-1.5 additionally stabilizes the low-temperature regime, ensuring convergence to the classical solution while maintaining smooth gradients throughout training.

Beyond the technical result, this formulation encourages a shift toward continuous versions of classical methods. Relying on strictly discrete pipelines often forces artificial separations between components, limiting the development of homogeneous models that operate coherently under a single optimization principle. By recasting classical algorithms in differentiable form, one can design architectures where methodological blocks interact naturally, share gradients, and evolve jointly, paving the way for integrated systems that are more stable, expressive, and theoretically unified.

7 Acknowledgements

We thank Gustavo de los Ríos Alatorre for computational support, and Luis Alberto Muñoz for the in-office discussions that significantly contributed to this work. We also owe Luis a seafood meal for the key ideas he provided. A personal thank-you to Nezhil Nieto for encouraging me (the main author) to write more papers and Sofia Alvarez for proofreading.

References

- Mohiuddin Ahmed, Raihan Seraj, and Syed Mohammed Shamsul Islam. The k-means algorithm: A comprehensive survey and performance evaluation. *Electronics*, 9(8):1295, 2020.
- David Arthur and Sergei Vassilvitskii. k-means++: The advantages of careful seeding. Technical report, Stanford, 2006a.
- David Arthur and Sergei Vassilvitskii. How slow is the k-means method? In *Proceedings of the twenty-second annual symposium on Computational geometry*, pages 144–153, 2006b.
- Mohamed Ishmael Belghazi, Aristide Baratin, Sai Rajeshwar, Sherjil Ozair, Yoshua Bengio, Aaron Courville, and Devon Hjelm. Mutual information neural estimation. In *International conference on machine learning*, pages 531–540. PMLR, 2018.
- Johannes Blömer, Christiane Lammersen, Melanie Schmidt, and Christian Sohler. Theoretical analysis of the k-means algorithm—a survey. In *Algorithm Engineering: Selected Results and Surveys*, pages 81–116. Springer, 2016.
- Mathilde Caron, Piotr Bojanowski, Armand Joulin, and Matthijs Douze. Deep clustering for unsupervised learning of visual features. In *Proceedings of the European conference on computer vision (ECCV)*, pages 132–149, 2018.
- M. Emre Celebi, Hassan A. Kingravi, and Patricio A. Vela. A comparative study of efficient initialization methods for the k-means clustering algorithm. *Expert Systems with Applications*, 40(1):200–210, January 2013. ISSN 0957-4174. doi: 10.1016/j.eswa.2012.07.021. URL <http://dx.doi.org/10.1016/j.eswa.2012.07.021>.
- Gianni Dal Maso. *An introduction to Γ -convergence*, volume 8. Springer Science & Business Media, 2012.
- Felipe de Jesús Félix Arredondo, Nezhil Nieto Gutiérrez, Gustavo De Los Ríos Alatorre, Arturo José Murra López, Manuel Alejandro Ucan-Puc, and Luis Alberto Muñoz Ubando. Deep mutual information meets segmentation: Enhancing neural network segmentation via mutual information regularization. In *Mexican International Conference on Artificial Intelligence*, pages 289–302. Springer, 2025.
- Inderjit S Dhillon, Yuqiang Guan, and Brian Kulis. Kernel k-means: spectral clustering and normalized cuts. In *Proceedings of the tenth ACM SIGKDD international conference on Knowledge discovery and data mining*, pages 551–556, 2004.
- KM Faraoun and Aoued Boukelif. Neural networks learning improvement using the k-means clustering algorithm to detect network intrusions. *INFOCOMP Journal of Computer Science*, 5(3):28–36, 2006.

- Boyan Gao, Yongxin Yang, Henry Gouk, and Timothy M Hospedales. Deep clustering with concrete k-means. In *ICASSP 2020-2020 IEEE international conference on acoustics, speech and signal processing (ICASSP)*, pages 4252–4256. IEEE, 2020.
- Quanxue Gao, Qianqian Wang, Han Lu, Wei Xia, and Xinbo Gao. Rethinking k-means from manifold learning perspective. *arXiv preprint arXiv:2305.07213*, 2023.
- Sinuhé Ginés-Palestino, Eduardo Roldán-Reyes, Marcela Quiroz-Castellanos, and Adilene Palma Asunción. Improving k-means algorithm performance through an ant colony optimization strategy. In *Mexican International Conference on Artificial Intelligence*, pages 194–203. Springer, 2025.
- Ian Goodfellow. Deep learning, 2016.
- Trevor Hastie, Robert Tibshirani, Jerome Friedman, and James Franklin. The elements of statistical learning: data mining, inference and prediction. *The Mathematical Intelligencer*, 27(2):83–85, 2005.
- Tapas Kanungo, David M Mount, Nathan S Netanyahu, Christine D Piatko, Ruth Silverman, and Angela Y Wu. An efficient k-means clustering algorithm: Analysis and implementation. *IEEE transactions on pattern analysis and machine intelligence*, 24(7):881–892, 2002.
- David Lowe and D Broomhead. Multivariable functional interpolation and adaptive networks. *Complex systems*, 2(3):321–355, 1988.
- Jörg Lücke and Dennis Forster. k-means as a variational em approximation of gaussian mixture models. *Pattern Recognition Letters*, 125:349–356, 2019.
- John Moody and Christian J Darken. Fast learning in networks of locally-tuned processing units. *Neural computation*, 1(2):281–294, 1989.
- Jooyoung Park and Irwin W Sandberg. Universal approximation using radial-basis-function networks. *Neural computation*, 3(2):246–257, 1991.
- Ben Peters, Vlad Niculae, and André FT Martins. Sparse sequence-to-sequence models. *arXiv preprint arXiv:1905.05702*, 2019.
- Qichao Que and Mikhail Belkin. Back to the future: Radial basis function networks revisited. In *Artificial intelligence and statistics*, pages 1375–1383. PMLR, 2016.
- Yordan P Raykov, Alexis Boukouvalas, Fahd Baig, and Max A Little. What to do when k-means clustering fails: a simple yet principled alternative algorithm. *PloS one*, 11(9):e0162259, 2016.
- Erich Schubert. Stop using the elbow criterion for k-means and how to choose the number of clusters instead. *ACM SIGKDD Explorations Newsletter*, 25(1):36–42, 2023.
- Matus Telgarsky and Andrea Vattani. Hartigan’s method: k-means clustering without voronoi. In *Proceedings of the thirteenth international conference on artificial intelligence and statistics*, pages 820–827. JMLR Workshop and Conference Proceedings, 2010.
- Yuriy Ushenko, Victoria Vysotska, Daryna Zadorozhna, Mariia Spodaryk, Zhengbing Hu, and Dmytro Uhryn. Agile technology of information data engineering for intelligent analysis of the happiness index and life satisfaction in known world cities. *International Journal of Information Engineering and Electronic Business*, 17(3):99–153, 2025. doi: 10.5815/ijieeb.2025.03.07.
- Lei Xu and Michael I Jordan. On convergence properties of the em algorithm for gaussian mixtures. *Neural computation*, 8(1):129–151, 1996.
- Jian Min Zhu, Peng Du, and Ting Ting Fu. Research for rbf neural networks modeling accuracy of determining the basis function center based on clustering methods. *Advanced Materials Research*, 317:1529–1536, 2011.

A Optional Proofs

A.1 Proof of Corollary 1 (Coercivity of the Theorem 1)

Corollary. Assume that J is coercive on $\mathbb{R}^{k \times d}$. Then the conclusion of Theorem 1 remains valid with $\mathcal{K} = \mathbb{R}^{k \times d}$.

Proof. Coercivity of J implies that its sublevel sets are bounded. Since $\mathcal{L}_{\sigma_m} \rightarrow J$ pointwise and $\mathcal{L}_{\sigma_m} \geq 0$, minimizers of \mathcal{L}_{σ_m} remain in a common bounded sublevel set. Hence minimizing sequences are precompact, and the argument of Theorem 1 applies on this bounded set. The conclusion follows. \square

A.2 Proof of Theorem 5 (Hard-Assignment Limit of Entmax-1.5/Softmax)

Let $d_{ij} = \|x_i - \mu_j\|^2$ and, for $\tau > 0$, define the negative-logit vectors

$$z_i(\tau) = -\frac{1}{\tau} (d_{i1}, \dots, d_{ik}) \in \mathbb{R}^k.$$

For $\alpha \geq 1$, the Entmax- α transformation is the solution of the variational problem

$$\text{Entmax}_\alpha(z) = \arg \max_{p \in \Delta^{k-1}} (p^\top z + H_\alpha(p)),$$

where $H_\alpha(p)$ denotes the Tsallis entropy of order α . For $\alpha = 1$, this recovers the usual Softmax.

Theorem 5. For any $\alpha \in [1, 2]$ and all i ,

$$r_{ij}^{(\alpha, \tau)} := (\text{Entmax}_\alpha(z_i(\tau)))_j \longrightarrow r_{ij}(0) = \mathbf{1}\left\{j = \arg \min_\ell d_{i\ell}\right\} \quad \text{pointwise as } \tau \rightarrow 0^+.$$

If the minimizer of $d_{i\ell}$ is unique, the limit is the corresponding one-hot vector.

Proof. As $\tau \rightarrow 0^+$, the coordinates of $z_i(\tau)$ separate in magnitude:

$$z_{i\ell^*}(\tau) \gg z_{ij}(\tau) \quad \text{for } \ell^* = \arg \min_\ell d_{i\ell}, j \neq \ell^*.$$

In the variational characterization of entmax- α , the linear term $p^\top z_i(\tau)$ scales as $1/\tau$, while $H_\alpha(p)$ stays bounded independently of τ . Thus, for sufficiently small τ , the linear term dominates and the maximizer must concentrate its mass on the coordinates that maximize $z_i(\tau)$, i.e., those minimizing d_{ij} .

Formally,

$$\frac{1}{\tau} p^\top (-d_i) \gg H_\alpha(p) \implies \text{Entmax}_\alpha(z_i(\tau)) \in \arg \max_{p \in \Delta^{k-1}} p^\top z_i(\tau).$$

The maximizers of a linear functional over the simplex are precisely the extreme points supported on the coordinates where the maximum is achieved. If the maximum is unique, the solution is the one-hot vector at ℓ^* ; if ties exist, Entmax- α spreads mass only among tied coordinates.

By pointwise continuity of the convex problem and the dominance of the linear term, we obtain

$$r_{ij}^{(\alpha, \tau)} \xrightarrow{\tau \rightarrow 0^+} r_{ij}(0),$$

with the additional sparsity property characteristic of $\alpha > 1$, such as Entmax-1.5. \square

B Algorithms for the clustering

B.1 K-Means

Algorithm 1 K-Means Algorithmic procedure for standard K-Means with k clusters and T iterations. At each step, points are reassigned to the nearest centroid and centroids are recomputed as arithmetic means of their assigned sets.

Require: Dataset $X \in \mathbb{R}^{n \times d}$, clusters k , iterations T

```
1: Initialize  $\mu \leftarrow \text{InitCenters}(X, k)$ 
2: for  $t = 1, \dots, T$  do
3:   Compute squared distances  $D_{ij} = \|x_i - \mu_j\|^2$ 
4:   Assign clusters  $S_i = \arg \min_j D_{ij}$ 
5:   for  $j = 1, \dots, k$  do
6:      $X_j \leftarrow \{x_i : S_i = j\}$ 
7:     if  $|X_j| > 0$  then
8:        $\mu_j \leftarrow \frac{1}{|X_j|} \sum_{x \in X_j} x$ 
9:     end if
10:  end for
11: end for
12: return  $(\mu, S)$ 
```

B.2 SoftRBF

Algorithm 2 SoftRBF-Net: Soft K-Means optimization using RBF-based similarity and Entmax-1.5 assignments. Centroid updates are performed via a closed-form gradient descent step with an adaptive learning rate $\eta_j = 1/(2r_j)$ for each cluster, where $r_j = \sum_i R_{ij}$.

Require: Dataset $X \in \mathbb{R}^{n \times d}$, clusters k , scale σ , iterations T

```
Initialize  $\mu \leftarrow \text{InitCenters}(X, k)$ 
2: for  $t = 1, \dots, T$  do
   Compute squared distances  $D_{ij} = \|x_i - \mu_j\|^2$ 
4:   Compute logits  $Z_{ij} = -D_{ij}/(2\sigma^2)$  ▷ Ensuring consistency with Eq. 7
   Compute soft assignments  $R = \text{Entmax}_{1.5}(Z)$ 
6:    $r_j = \sum_{i=1}^n R_{ij}$  ▷ Cluster mass / Responsibility sum
    $w_j = \sum_{i=1}^n R_{ij} x_i$  ▷ Weighted sum of points
8:   for  $j = 1, \dots, k$  do
     Gradient:  $\nabla_j = 2(r_j \mu_j - w_j)$ 
10:    Step size:  $\eta_j = 1/(2r_j)$ 
     Update:  $\mu_j \leftarrow \mu_j - \eta_j \nabla_j$ 
12:   end for
   end for
14: return  $(\mu, R)$ 
```

C Algorithms for evaluation

C.1 With fixed initialization

Algorithm 3 Evaluation of the convergence metric $R_{\text{fixed}}(\sigma)$, where the same set of M initial centroid configurations is used for every value of σ . This experiment isolates the effect of the RBF temperature parameter by holding initialization variability fixed across all runs.

Require: Data matrix X , number of clusters k , iterations T , number of initializations M

Require: Sigma range $\{\sigma_1, \dots, \sigma_L\}$

```
1: Generate  $\{\mu_1^{(0)}, \dots, \mu_M^{(0)}\}$  using  $M$  random initializations
2: Run K-Means for each  $\mu_i^{(0)}$ :
3: for  $i = 1 \dots M$  do
4:    $\mu_i^{\text{KM}} \leftarrow \text{KMeans}(X, \mu_i^{(0)})$ 
5: end for
6: for  $\ell = 1 \dots L$  do
7:    $\sigma \leftarrow \sigma_\ell$ 
8:   Initialize list  $\mathcal{D} = []$ 
9:   for  $i = 1 \dots M$  do
10:     $\mu_{i,\sigma}^{\text{soft}} \leftarrow \text{SoftKMeansRBFGrad}(X, \mu_i^{(0)}, \sigma)$ 
11:    Compute optimal permutation  $\pi$  matching centroids
12:     $d_i \leftarrow \sum_{j=1}^k \left\| \mu_{i,j}^{\text{KM}} - \mu_{i,\sigma,\pi(j)}^{\text{soft}} \right\|$ 
13:    Append  $d_i$  to  $\mathcal{D}$ 
14:   end for
15:    $R_{\text{fixed}}(\sigma_\ell) \leftarrow \text{mean}(\mathcal{D})$ 
16: end for
17: return  $\{R_{\text{fixed}}(\sigma_1), \dots, R_{\text{fixed}}(\sigma_L)\}$ 
```

C.2 With variable initialization

Algorithm 4 Evaluation of the convergence metric $R_{\text{resampled}}(\sigma)$, where fresh random initial centroid configurations are drawn independently for each value of σ . This experiment captures both initialization variability and the smoothing effect of σ , producing an initialization-averaged convergence curve.

Require: Data matrix X , number of clusters k , iterations T , number of samples M

Require: Sigma range $\{\sigma_1, \dots, \sigma_L\}$

```
1: for  $\ell = 1 \dots L$  do
2:    $\sigma \leftarrow \sigma_\ell$ 
3:   Initialize list  $\mathcal{D} = \{\}$ 
4:   for  $i = 1 \dots M$  do
5:     Draw a fresh initialization  $\mu^{(0)}$ 
6:      $\mu^{\text{KM}} \leftarrow \text{KMeans}(X, \mu^{(0)})$ 
7:      $\mu^{\text{soft}} \leftarrow \text{SoftKMeansRBFGrad}(X, \mu^{(0)}, \sigma)$ 
8:     Compute optimal permutation  $\pi$ 
9:      $d_i \leftarrow \sum_{j=1}^k \left\| \mu_j^{\text{KM}} - \mu_{\pi(j)}^{\text{soft}} \right\|$ 
10:    Append  $d_i$  to  $\mathcal{D}$ 
11:   end for
12:    $R_{\text{resampled}}(\sigma_\ell) \leftarrow \text{mean}(\mathcal{D})$ 
13: end for
14: return  $\{R_{\text{resampled}}(\sigma_1), \dots, R_{\text{resampled}}(\sigma_L)\}$ 
```
